Implementation of the water ice cloud microphysics interactive with the dust cycle into DRAMATIC MGCM

T. Kuroda[1], **M. Kobayashi**[1,2], **A. Kamada**[1,3], **H. Karyu**[1,4,5], **R. Sato**[1], and **N. Sugimoto**[6], [1]*Department of Geophysics, Graduate School of Science, Tohoku University, Sendai, Japan (tkuroda@tohoku.ac.jp),* [2] *Laboratoire de Météorologie Dynamique/Institut Pierre Simon Laplace (LMD/IPSL), Sorbonne Université, Paris, France,* [3]*Earth-Life Science Institute, Institute of Science Tokyo, Tokyo, Japan,* [4]*Royal Belgian Institute for Space Aeronomy (BIRA-IASB), Brussels, Belgium,* [5]*Earth and Life Institute, Université Catholique de Louvain, Louvain, Belgium,* [6]*Department of Physics, Keio University, Yokohama, Japan*

Introduction:

The DRAMATIC (Dynamics, RAdiation, MAterial Transport, and their mutual Interactions) Mars Global Climate Model (MGCM) has long been used to investigate atmospheric dynamics and material transport on Mars [1-3], including the facilitation of the collaborations with observational data and future mission plannings [4,5]. Recently it reproduced the interactions between the atmosphere and subsurface water by implementing the adsorption properties of regolith [6].

However, about the atmopheric water cycle, it only had a cloud formation scheme with simple estimations of number density and size of dust nuclei [6-8], which was not interactive with realistic dust cycle. Now we have considerably updated the water cycle scheme in the DRAMATIC MGCM, newly implementing the realistic cloud microphysics interactive with the dust cycle for 6 particle sizes. Here we show several quick results with the new scheme, and in the presentation we plan to show further discussions including the comparisons with the observational data.

This development will contribute to the atmospheric observations of Mars by the Japanese mission MMX (Martial Moons eXplanation) [9] launching in 2026. Moreover, it should link to the improvements of atmospheric simulations of Mars in various ages, for the investigations of the evolution of its water environment and climate.

Methods:

The current version of the MGCM is based on MIROC6 [10], and we have updated the vertical layers to use a hybrid sigma-pressure coordinate. Now we have implemented a dust cycle featuring 6 particle mode radii (0.0625, 0.125, 0.25, 0.5, 1, and 2 μm). Dust is injected from the surface according to three-dimensional scenarios (latitude, longitude, and time) based on past observations of opacity [11,12], with the ratios of each mode radius consistently with past observations (effective radius of 1.6 μm and variance of 0.2 [13]). The airborne dust also serves as nuclei for the formation of water ice clouds. The microphysics governing the formation of water ice clouds is newly implemented based on the theory of heterogeneous nucletion with spherical solid nuclei [14-16], as has been implemented in a preceding work [17]. The sources of atmospheric water are polar ice caps in both hemispheres, defining regions with the daytime thermal inertia of >1000 J m^{-2} K^{-1} $s^{-1/2}$ in the dataset [18].

We also have newly implemented the radiative effects of water ice clouds, CO_2 ice clouds, and water vapor, as well as those of CO_2 gas and dust particles classically implemented. Atmospheric raditation is calculated with 26 bands between 10 and 115000 cm^{-1} in wavenumber (0.087 and 1000 μm in wavelength), and the simulated opacities shown in Results represent the outputs at corresponding bands.

Here we show the results with the horizontal resolution of T42 (~2.8° for both latitude and longitude), and vertical 34 layers with the top altitude of ~87 km (~0.1 Pa). The "climatology" dust opacity scenario [19] is implemeneted.

Results:

Figure 1 shows the annual-latitudinal cross sections of simulated daytime (2pm) water vapor column density (in pr.μm) and water ice cloud column opacity in infrared (at 825 cm^{-1}) in the 15th year from isothermal and dry (no water vapor/ice in the atmosphere) state. Those results well reproduce the MGS/TES observation [20] in overall. The water ice opacity in near-infrared (at 3.4 μm corresponding to the MRO/CRISM observation [21]) is almost the same as in infrared, and the opacity in ultravioler (at 320 nm corrsponding to the MRO/MARCI observation [22]) is slightry smaller than in infrared/near-infrared.

Figures 2, 3, and 4 show the latitude-altitude cross sections of simulated daytime (3pm) and nighttime (3am) temperature, water ice cloud opacity at 843 cm^{-1}, and dust opacity at 463 cm^{-1}, respectively. Those results well reproduce the MRO/MCS observation [23].

Figures 5 and 6 show the simulated latitude-altitude cross sections of the mean radius and variance of the water ice clouds and dust particles, respectively. Those are quick results, and the detailed investigations of the particle size distributions of water ice and airborne dust will be shown in the presentation.

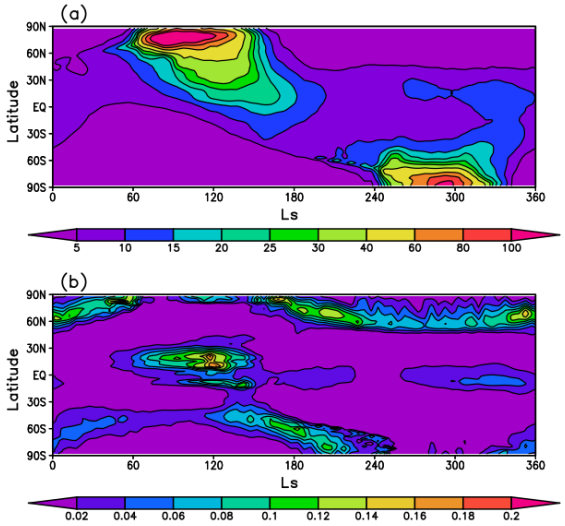

Figure 1: Seasonal and latitudinal distributions of simulated (a) daytime (2pm) water vapor column density (in pr.µm) and (b) water ice cloud column opacity at 825 cm^{-1}.

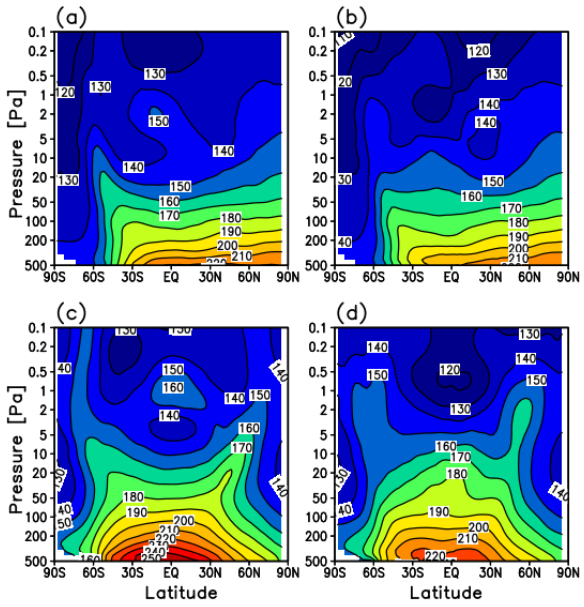

Figure 2: Latitude-altitude cross sections of simulated zonal-mean temperature (in K) for (a) daytime (3pm) at L_s=90° (northern summer solstice), (b) nighttime (3am) at L_s=90°, (c) daytime at L_s=180° (northern autumn equinox), and (d) nighttime at L_s=180°.

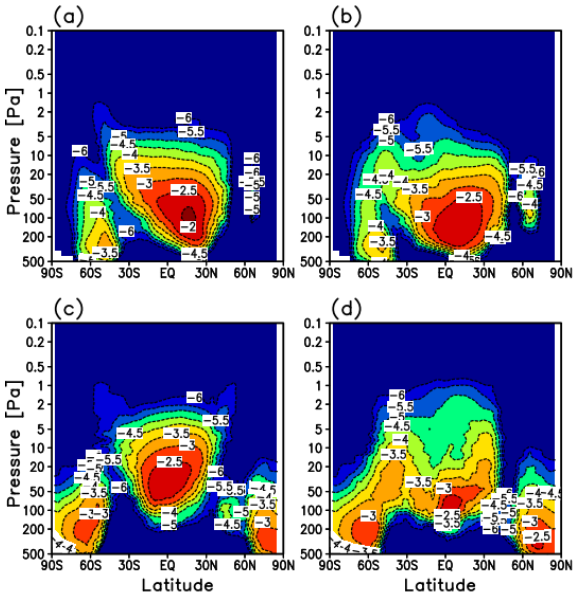

Figure 3: Same as Figure 2, except $\log_{10}$ of water ice cloud opacity at 843 cm^{-1} (in km^{-1}).

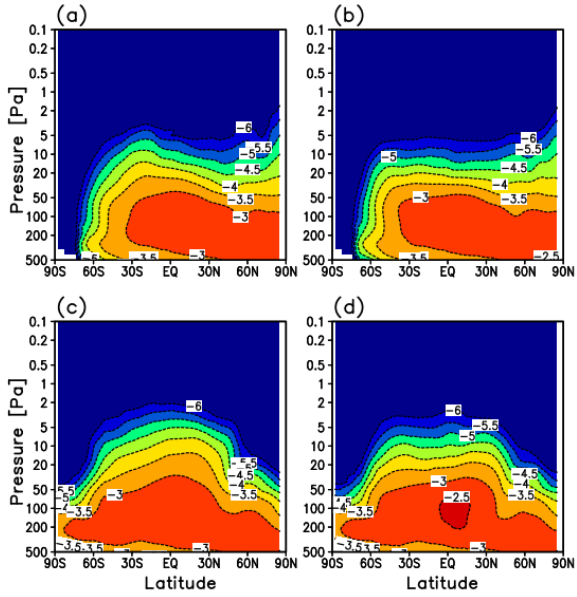

Figure 4: Same as Figure 2, except $\log_{10}$ of dust opacity at 463 cm^{-1} (in km^{-1}).

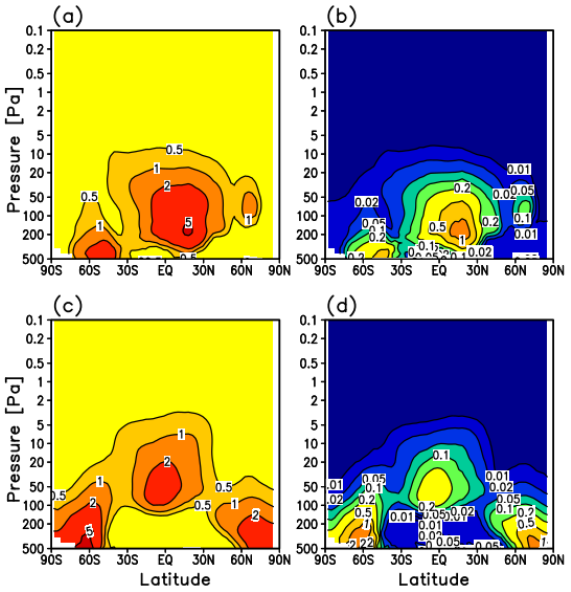

Figure 5: Latitude-altitude cross sections of simulated zonal-mean water ice cloud properties: (a) mean radius (in μm) at L_s=90°, (b) variance (×10^{-6}) at L_s=90°, (c) mean radius at L_s=180°, and (d) variance at L_s=180°.

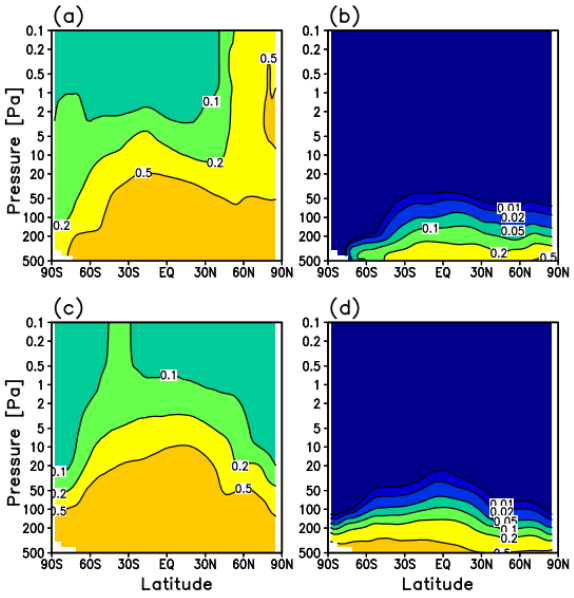

Figure 6: Same as Figure 5, except airborne dust.

References:

[1] Kuroda, T. et al. (2005), Simulation of the Martian Atmosphere Using a CCSR/NIES AGCM. *Journal of the Meteorological Society of Japan*, **83**, 1–19.

[2] Kuroda, T. et al. (2013), Carbon dioxide ice clouds, snowfalls, and baroclinic waves in the northern winter polar atmosphere of Mars, *Geophysical Research Letters,* **40**, 1484–1488.

[3] Kuroda, T. et al. (2015), A global view of gravity waves in the Martian atmosphere inferred from a high-resolution general circulation model. *Geophysical Research Letters,* **42**, 9213–9222.

[4] Miyamoto, A. et al. (2021), Intense Zonal Wind in the Martian Mesosphere During the 2018 Planet-Encircling Dust Event Observed by Ground-based IR Heterodyne Spectroscopy. *Geophysical Research Letters*, **48**, e2021GL092413.

[5] Kurokawa, H. et al. (2022), Can we constrain the origin of Mars' recurring slope lineae using atmospheric observations? *Icarus*, **371**, 114688.

[6] Kobayashi, M. et al. (2025), Large Water Inventory in Highly Adsorptive Regolith Simulated With a Mars Global Climate Model. *Journal of Geophysical Research Planets*, **130**, e2024JE008697.

[7] Kuroda, T. (2017), Simulation of the Water Cycle Including HDO/H_2O Isotopic Fractionation on the Present Mars Using DRAMATIC MGCM, *Sixth international workshop on the Mars atmosphere: modelling and observations*, LMD, CNES and IAA.

[8] Montmessin, F. et al. (2004), Origin and role of water ice clouds in the Martian water cycle as inferred from a general circulation model, *Journal of Geophysical Research*, **109**, E10004.

[9] Ogohara, K. et al. (2022), The Mars system revealed by the Martian Moons eXploration mission, *Earth, Planets and Space*, **74**, 1.

[10] Tatebe, H. et al. (2019), Description and basic evaluation of simulated mean state, internal variability, and climate sensitivity in MIROC6, *Geoscientific Model Development*, **12**, 2727–2765.

[11] Montabine, L. et al. (2015), Eight-year climatology of dust optical depth on Mars, *Icarus*, **251**, 65–95.

[12] Montabine, L. et al. (2020), Martian Year 34 Column Dust Climatology from Mars Climate Sounder Observations: Reconstructed Maps and Model Simulations, *Journal of Geophysical Research Planets*, **125**, e2019JE006111.

[13] Tomasko, M.G. et al. (1999), Properties of dust in the Martian atmosphere from the Imager on Mars Pathfinder, *Journal of Geophysical Research*, **104**, 8987–9007.

[14] Keesee, R.G. (1989), Nucleation and particle formation in the upper atmosphere, *Journal of Geophysical Research*, **94**, 14683–14692.

[15] Montmessin, F. et al. (2002), New insights into Martian dust distribution and water-ice cloud microphysics, *Journal of Geophysical Research*, **107**, 5037.

[16] Jacobson, M.Z. (2005), Fundamentals of Atmospheric Modeling, Cambridge University Press.

[17] Navarro, T. et al. (2014), Global climate modeling of the Martian water cycle with improvedmicrophysics andradiatively active water ice clouds, *Journal of Geophysical Research Planets*, **119**, 1479–1495.
[18] Putzig, N., & Mellon, M. (2007), Apparent thermal inertia and the surface heterogeneity of Mars, *Icarus*, **191**, 68–94.
[19] Millour, E. et al. (2018), The Mars Climate Database (Version 5.3), *Scientific Workshop: "From Mars Express to ExoMars"*, ESA-ESAC & IAA-CSIC.
[20] Smith, M.D. (2008), Spacecraft Observations of the Martian Atmosphere, *Annual Review of Earth and Planetary Sciences*, **36**, 191–219.
[21] Khayat, A.S.J. et al. (2023), The Mars Atmosphere Water Ice Aerosol Climatology by MRO/CRISM: 5 Mars Years of Observations, *Journal of Geophysical Research Planets*, **128**, e2023JE007761.
[22] Wolff, M.J. et al. (2019), Mapping water ice clouds on Mars with MRO/MARCI, *Icarus*, **332**, 24–49.
[23] McCleese, D.J. et al. (2010), Structure and dynamics of the Martian lower and middle atmosphere as observed by the Mars Climate Sounder: Seasonal variations in zonal mean temperature, dust, and water ice aerosols, *Journal of Geophysical Research*, **115**, E12016.